PERGAMON

International Journal of Heat and Mass Transfer 45 (2002) 3491–3501

International Journal of HEAT and MASS TRANSFER

www.elsevier.com/locate/ijhmt

A transient liquid crystal method using a 3-D inverse transient conduction scheme

Mingjie Lin [a], Ting Wang [b,*]

[a] Department of Mechanical Engineering, Clemson University, Clemson, SC 29634-0921, USA
[b] Energy Conversion and Conservation Center, University of New Orleans, New Orleans, LA 70148-2220, USA

Received 28 September 2001; received in revised form 8 February 2002

Abstract

The present method utilized the hue-angle method to process the color images captured from the liquid crystal color play. Instantaneous temperature readings from embedded thermocouples were utilized for in situ calibration of hue angle for each data set. The convective heat transfer coefficient results were obtained by performing a 3-D inverse transient conduction calculation over the entire jet impingement target surface and the substrate. The results of average heat transfer coefficients agreed well with previous experimental results of point measurements by thermocouples.

Comparison between 1-D and 3-D results indicates that 1-D results are higher than the 3-D results with the local maximum and minimum heat transfer values being overvalued by about 15–20% and the overall heat transfer by approximately 12%. This is due to the fact that 1-D method does not include the lateral heat flows induced by local temperature gradients.

Keywords: Inverse transient scheme; Transient liquid crystal scheme; Hue angle; Impingement jets

1. Introduction

The primary motivations of employing liquid crystal were: (a) liquid crystal method can make detailed surface mapping of heat transfer performance, (b) liquid crystal method is more economical and affordable than infrared thermal imaging method. However, for commercially available thermochromic liquid crystal (TLC) products, the color play range is typically only about 5 °C, which is limited and undesirable for most practical applications. Generally, the liquid crystal method can be classified into two categories: steady method and transient method.

1.1. Steady TLC method

The steady TLC method allows the entire surface to be mapped from one TLC image using a color processing system. Numerous studies have been conducted using steady TLC method including Ferguson [1], Den Ouden and Hoogendoorn [2], Cooper et al. [3], Goldstein and Timmers [4], Akino et al. [5], Baughn et al. [6], etc.

Simonich and Maffat [7] used a TLC paint with one active temperature range and employed an optically filtered mercury lamp to tailor the wave length of the incident light to enhance the brightness of a selected color band. Hippensteele et al. [8] calibrated on the yellow band observed in white light and adjusted the heat flux into the surface so the position of the yellow band over a series of images mapped out the heat coefficient over the surface.

To reduce the uncertainty produced by human eye observation, Arkno et al. [9] and Hollingsworth et al. [10] both proposed a trichromic decomposition method, which is a way of determining the temperature of a liquid crystal surface from a quantitative measurement of its color. Camci et al. [11] proposed a time efficient hue capturing technique to interpret TLC images.

2. Transient TLC method

To overcome the problems of limited color play range and deteriorating characteristic of color play

* Corresponding author. Tel.: +1-504-280-7183; fax: +1-504-280-5539.
E-mail address: twang@uno.edu (T. Wang).

0017-9310/02/$ - see front matter
PII: S0017-9310(02)00073-X

Nomenclature

d	jet hole diameter
h	local heat transfer coefficient
H	average heat transfer coefficient
k	air thermal conductivity
Nu	Nusselt number (hd/k)
Re	Reynolds number (Vd/v)
RGB	Red, green, and blue
T	temperature
TLC	thermochromic liquid crystal
V	jet velocity
v	air kinematic viscosity

Subscripts

jet	impingement jet
max	maximum value
min	minimum value

encountered in steady state TLC method, various transient TLC methods were developed by applying a semi-infinite transient experimental technique to study the heat transfer performance on a flat test surface. The transient method is based on the fact that when the test surface of a uniform initial temperature is suddenly exposed to a uniformly heated or cooled flow, the magnitudes of the time-varying surface temperature is governed by transient heat conduction penetrating into a semi-infinite solid. The details of this method can be found in the paper by Ireland and Jones [12].

Metzger et al. [13] conducted a transient TLC approach to study jet impingement cooling on a rotating disk. Humber and Viskanta [14] used the similar transient TLC method to examine the influence of spent air exits located between the jets on the magnitude and uniformity of local heat transfer coefficient for a confined 3×3 square array of axis-symmetric air jets impinging normally to a heated surface. Chyu et al. [15] have utilized bulk mean temperature to refine the TLC method for turbine foil internal passage cooling.

Theoretically, the following conditions need to be satisfied for employing the analytical 1-D transient solutions: (a) 1-D heat conduction, (b) imposing an instantaneous convective heating or cooling boundary condition on the surface, and (c) semi-infinite depth of the solid. Among these conditions, condition (a) is frequently violated by nearly all the applications. To satisfy conditions (b) and (c), inconvenient and/or complex designs are frequently required to be implemented. For example, in practical experiment cases, the ideal step temperature change on the test surface is not achievable. To deal with it, one must use a superimposed method to approximate the transient temperature changing curve on the test surface by integrating a finite number of step changes (see [16]). Depending on the time step size, the obtained data accuracy may not always be satisfying.

Motivated by the needs for more accurately measuring the heat transfer coefficients and for simplifying experimental setup and procedures, this paper develops an approach of coupling the transient liquid crystal method with a 3-D inverse transient conduction scheme. A jet impingement test rig was employed to produce non-uniform surface heat transfer coefficient for this study.

3. Experimental program

3.1. Test section

In the present test section, as shown in Fig. 1, flow from the compressor first came through the inlet and entered the chamber A, then flowed through the in-lined, uniformly distributed impingement holes on the aluminum plate and impinged on the heated target surface. A specially designed composite heated test surface employing the TLC method is illustrated in Fig 1. The test surface consisted of five layers. The first layer was a clear LEXAN plate of 12.6 mm (1/2 in.) thick which served as the support for the heater and the liquid crystal sheet. The second layer was the liquid crystal sheet, which was about 0.1 mm thick with adhesive on both sides. The liquid crystal sheet (model number R25C5, HALLCREST) had a temperature range of 25–30 °C. The third, fourth, and fifth layers were the heater sandwiched between silicon rubber layers 0.47 mm thick on both

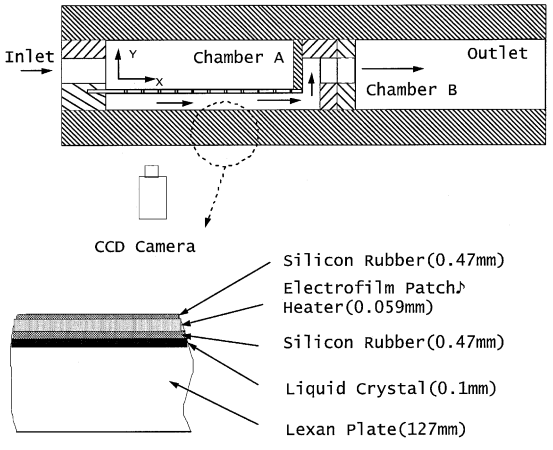

Fig. 1. Test section and the composition of the heated wall.

sides. The total thickness of the patch heater was approximately 1 mm and the actual thickness of etched heating foil was about 0.059 mm.

In the present test section, if the method of using analytical 1-D transient conduction solutions were adopted, an instantaneous step-change of heated flow would have to be satisfied. In the current study, the impingement air flowed through an aluminum plate drilled with impingement jet holes, so the jet air temperature would be cooled by the aluminum plate initially and could not provide an adequate step change. Furthermore, steep lateral temperature gradients on the jet impingement surface would introduce errors due to deviation from 1-D assumption. Therefore, instead of imposing a step change of the heated air jet impinging on a cold target surface, the experimental condition in this study was designed to use a step-changed heated target surface with steady, cold air jets. Since the heater was very close to the cooling surface (within 1 mm), the heat transfer from the heater to raise the cooling surface 5 °C was estimated to be 20 ms, which was one order of magnitude faster than the time (0.3 s) needed for step-changing the flow temperature. Furthermore, providing a step-change of surface heat flux is more convenient than step-changing the main flow temperature. Considering the situations encountered in this study, no analytical heat conduction solutions were available for the present transient liquid crystal method. Therefore, the following approach was developed by this study to combine the transient TLC imaging techniques with a 3-D inverse transient heat conduction scheme to obtain the surface heat transfer coefficients.

4. Image processing system

The image processing procedure is shown in the upper part of Fig. 2. First, a period of TLC color images on the test surface was recorded by a standard 8 mm camcorder. Then images were digitized to TIFF format. The image acquisition rate was set to be 30 images per second, which was the standard image recording rate of the majority of CCD cameras. The whole TLC color play history became a large number of discrete image TIFF files. Using MATLAB image processing toolbox, each pixel of those images could be interpreted as a (R, G, B) data set. (R, G, B) represents the color intensity value of the three primary colors: red, green, and blue. The next step was to transform the color information in the *RGB* domain into the *UVW* domain. The trichromatic decomposition method was employed to achieve this goal.

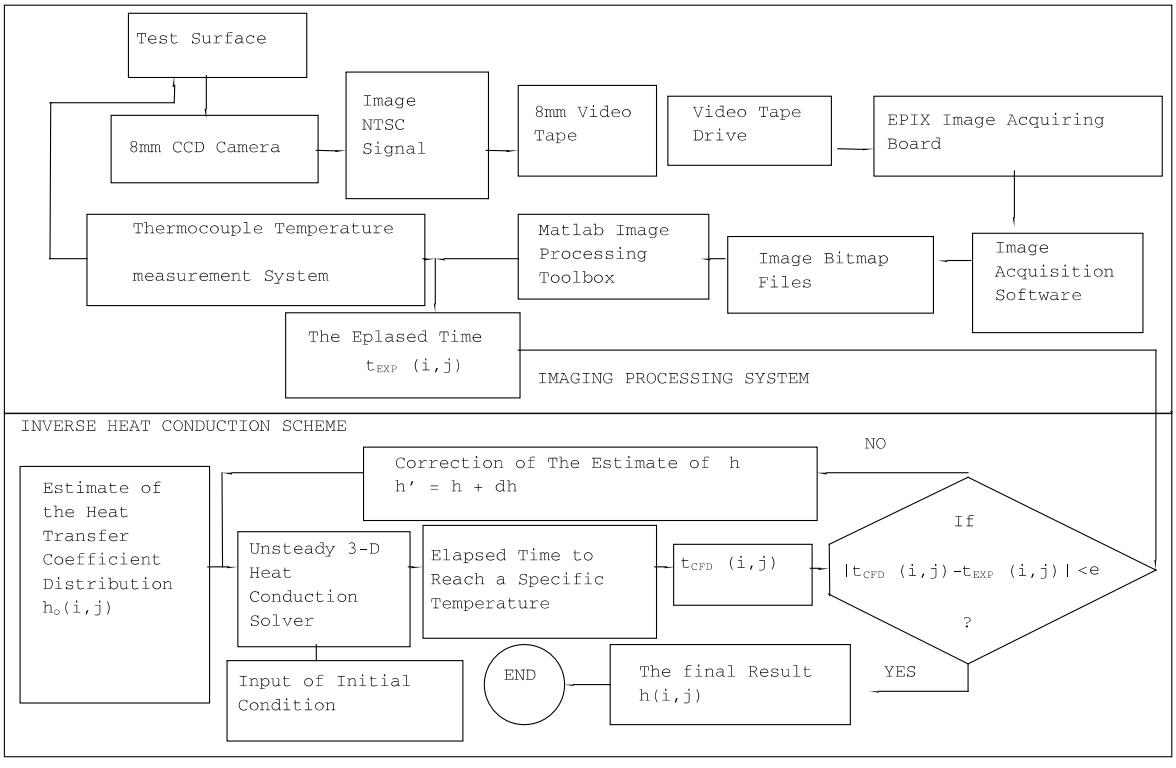

Fig. 2. Flow charts of the image processing system and the 3-D inverse transient conduction scheme.

4.1. Trichromic decomposition

The trichromic decomposition is a standard quantitative method to assign a scalar value to the perception of color. This method is based on the mathematical representation of color that is widely used by television and color printing industries. Sponson [17] and Pratt [18] published detailed discussions of trichromic color representation in their texts. The RGB system may be the most internationally recognized operating domain for color quantification; however, it is strongly non-linear. The UVW system was designed to minimize non-linearities and provide a more uniform response of the human eye to change in colors.

The goal of the analysis is to evaluate the images recorded by the video recording system and to produce a scalar description of colors, that could generate an *unambiguous* description of the temperature of liquid crystal. The linear transformation between the RGB system and the UVW system was through the following matrix [10]:

$$(UVW)^{\mathrm{T}} = \mathbf{A}(RGB)^{\mathrm{T}}, \tag{1}$$

where

$$\mathbf{A} = \begin{bmatrix} 0.405 & 0.116 & 0.133 \\ 0.299 & 0.587 & 0.114 \\ 0.145 & 0.827 & 0.627 \end{bmatrix}. \tag{2}$$

The 3×3 matrix $\mathbf{A}$ was determined by deriving a set of equations that described the color matching conditions using the two primaries system [10]. The fraction of the total intensity attributable to each of the UVW primaries is: $u = U/(U+V+W)$, $v = V/(U+V+W)$, and $w = W/(U+V+W)$. The variables u, v, and w are called "chromaticity coordinates". The vector (u, v) is a sufficient description of all three variables since w can be uniquely determined if u, v are known. Fig. 3 shows a 2-D representation of colors in $u - v$ coordinates. White light, a uniform mixture of all wave lengths, is located at coordinates (u_0, v_0), where $u_0 = 0.201$ and $v_0 = 0.307$. The triangle formed by the *RGB* primaries contains all the colors that can be reproduced by a video system. Any point on this surface can be described either by a pair of chromaticity coordinate (u, v) or by the color deviation vector $(u - u_0, v - v_0)$ from the white-light reference point (see Fig. 4). The vector provides two values: radius and angle. The magnitude of this vector represents the saturation and the angle describes the hue. The hue angle θ (counter-clockwise as positive) and the magnitude ρ are defined as:

$$\theta = \operatorname{arctg}\left(\frac{v - v_0}{u - u_0}\right), \tag{3}$$

$$\rho = \sqrt{(u - u_o)^2 + (v - v_o)^2}. \tag{4}$$

Typically, when temperature increases, the color from a liquid crystal changes from brown to yellow to green to blue. When the data acquired through a video system were plotted, a monotonic hue-angle increase was observed as temperature increased. As an illustration, the chromaticity of a point on the test surface from a calibration experiment is shown in Fig. 4. The hue-angle was replotted versus temperature as Sample A in Fig. 5, which shows that there is a well-described relationship between the temperature and color hue angle in the color play range. In this method, a hue angle was used as the indicator of a specific temperature. For example, in Fig. 5, the hue angle 200° corresponds to the temperature at 32 °C. Four samples at different locations as shown in Fig. 5 show the repeatability and uncertainty of this method.

The hue angle approach was proposed by Hollingsworth et al. [10] in a *steady state* heat transfer study. To our knowledge, the current experiment might be the first one to apply hue angle to the transient TLC method. Another modification made to the previous transient

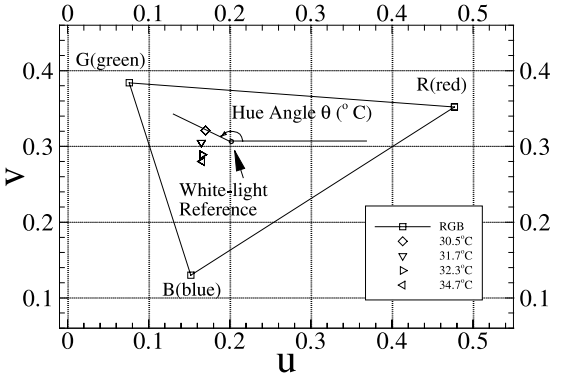

Fig. 3. Chromaticity diagram for the uniform chromaticity scale color system.

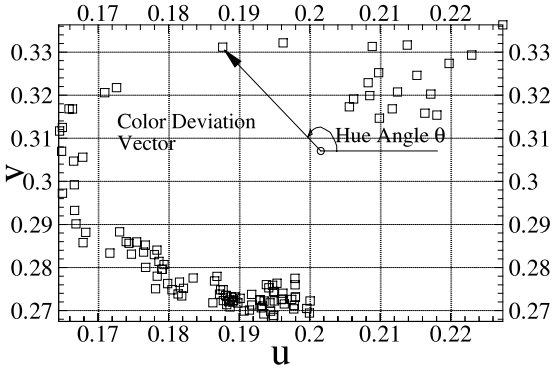

Fig. 4. Chromaticity of a TLC sample at different temperature levels.

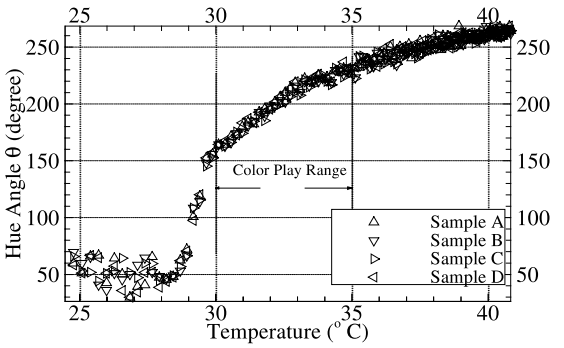

Fig. 5. Hue angle versus temperature of a TLC color history.

TLC method was instead of using pre-calibrated TLC color versus temperature characteristic, an in situ calibration by mapping actual thermocouple readings was performed during each experimental case.

After performing trichromic decomposition, all the TIFF image files were averaged into a sequential order of matrix with $(m \times n)$ entries, where m and n represent the number of pixels sampled in the x-direction and y-direction, respectively. The sequential order of those images also reflected the time history. One image file contained two types of information: the time elapse from the beginning of the experiment and target surface temperature distribution at that instant. For each image file at one instant, the image of the entire surface was transformed into a 3-D matrix $RGB\ (nx, ny, 3)$ by using the MATLAB image processing toolbox, where nx and ny stood for the number of pixels in x-direction and y-direction, respectively. From each pixel, the intensity value of each color, the RED, GREEN, and BLUE, was derived. By utilizing the linear transformation mentioned from before, the 3-D RGB matrix was further transformed into a 2-D matrix UV, from which the hue angle was calculated at each pixel of the image considered. After processing every image in this way, a large group of matrices was obtained in a time sequential order. For each pixel, the history of the hue angle change during the experiment was obtained. Referring to the hue-angle versus temperature curve as shown in Fig. 5, a particular data point which had demonstrated reliability and consistency between hue angle and the temperature was chosen as a reference point. For example, at the hue angle of 200°, the corresponding temperature was 32 °C. By looking through the hue angle's changing history, the time elapsed to reach the reference value (200°) could be obtained at each pixel. This elapsed time was calculated by multiplying the sequential number of the specific image by the time interval (1/30 s) between two successive images. Finally, a 2-D matrix $TIME\ (nx, ny, 1)$ containing the information of the duration for each pixel (or each physical location) on the target surface to reach a pre-determined temperature level (32 °C in the present study) could be obtained. At this stage, and for each case, the raw data had been reduced to a matrix $\tau(nx, ny)$, which stated the time period of each sampled pixel to reach the specific temperature level.

The next step of heat transfer data processing was to back calculate the heat transfer coefficient from the time elapse information. The 3-D inverse scheme was employed here. The temperature information obtained on the TLC surface was not on the true surface but a short distance beneath the surface. The unknown heat transfer coefficients were to be recovered as the boundary condition on the true surface of the heat conduction body. The dimensions and physical properties of the composite heated test surface and the heat flux generated by the heater were known. Using all these parameters as the input to the inverse scheme, the heat transfer coefficient at each location on the target surface could be calculated.

4.2. 3-D Inverse transient conduction scheme

For a transient heat conduction problem, the temperature distribution inside a solid can be found through numerical or analytical methods if the heat flux or temperature histories at the surface (i.e. the boundary conditions) of the solid are known. This is a direct problem. However, in many dynamic heat transfer situations, one of the boundary conditions, such as the surface heat flux or surface heat transfer coefficient, are not known, and they must be determined from transient temperature measurements at interior locations. This kind of problem is categorized as the inverse problem. In the present study, the term "inverse" was used to emphasize the nature of the current problem in a broad sense. In this study, the known information was the time period to reach a specific temperature for each pixel over the TLC surface beneath the heater, The unknown to be solved was the heat transfer coefficient distribution on the test surface. A program written in MATLAB was utilized to implement this scheme.

The inverse scheme consists of two stages. The first stage is to solve the direct heat conduction problem. The second stage is to correct the estimated heat transfer field. The heat transfer problem in this study is a 3-D transient heat conduction problem. The general governing equations for a 3-D transient conduction problem is:

$$\rho c \frac{\partial T}{\partial t} = \nabla \cdot (k \nabla T) + S, \tag{5}$$

where ρ is the local density of calculation domain, c is the local heat capacity of calculation domain,

$$\nabla : \frac{\partial}{\partial x} i + \frac{\partial}{\partial y} j + \frac{\partial}{\partial z} k$$

and S is the interior heat source.

The numerical calculation was performed using the second-order central differencing scheme for spatial axis and implicit method for temporal step. The discretization of the governing equation results in a large set of linear algebraic equations, which are solved by the Gauss–Seidel point-by-point iterative method. The results are deemed reaching convergence when the variation of consecutive results of at each grid point is less than 10^{-6}. After one round of solving a direct 3-D transient heat conduction problem, a predict-and-correct method is employed to adjust the input condition.

For this study, the inverse scheme starts with applying a guessed heat transfer coefficient distribution on the test surface as the boundary condition and compute the temperature field of the whole domain. The flow chart in the low part of Fig. 2 shows the procedure of the present inverse problem-solving scheme. The second step is to correct the previously guessed heat transfer coefficient distribution, and continue another run of 3-D transient heat transfer computation. This loop continues until the calculated transient temperature information (i.e. both time and temperature values) of each grid on the target surface matches the experimental data within the convergence criterion. During the correction process, the Newton root-finding method is adopted to correct the assumed heat transfer coefficient distribution as described below.

At the beginning of the correction loop, two estimates of h are given in such a way so that $h1$ is much smaller than the estimated value and the second value $h2$ is much larger. Therefore, h can be assured to be between $h1$ and $h2$, i.e. $h1 < h < h2$ (see Fig. 6). For each h, by computation, two values of t ($t1$ and $t2$) are obtained. The experimental results of t should be between $t1$ and $t2$. The next step is to obtain the next guess of h by utilizing the following formula:

$$h' = h1 + \frac{h2 - h1}{t2 - t1} \cdot (t - t1). \tag{6}$$

Using the corrected h' as the input, another resultant $h3$ can be obtained. If $h3$ is larger than $h, h1$ is replaced by the value of h'; otherwise, $h2$ is replaced by h'. Further on, using the new value of $h1$ and $h2$, repeat the whole calculation process until the relative difference between the calculated t and the experimental result t is within the acceptable tolerance, say 1×10^{-6} s, for each grid point on the target surface.

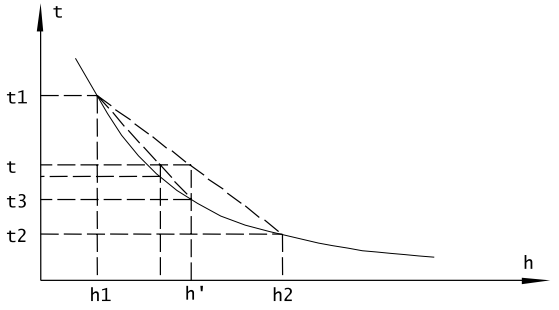

Fig. 6. Newton root-finding method to correct guessed heat transfer coefficient value.

To reveal the heat transfer characteristic details on the entire surface, the whole test surface was considered as the computational domain. Each of the composite layers of the heater was treated as an individual layer (two layers of silicon rubber, one layer of liquid crystal, and one layer of heating element). The heater was treated to generate energy uniformly by adding a source term to each of the computational grid. The grid system, as shown in Fig. 7, was $375(x) \times 240(y) \times 35(z)$, which was uniform in x- and z-directions and non-uniform in y-direction.

To determine the appropriate grid density, grid-independence tests have been performed. When the grid numbers changed from $187(x) \times 120(y) \times 17(z)$ to $375(x) \times 240(y) \times 35(z)$, the maximum relative deviation of the temperature was less than 2%, which was deemed acceptable to this study. No denser grid system was tried.

Generally, three kinds of boundary conditions are encountered in heat transfer conduction. These are: given boundary temperature (type I), given boundary heat flux (type II), and given surface heat transfer coefficient (type III).

On the front side (impingement side) of the test plate, the boundary condition is type III, but its value was unknown and was to be guessed first and corrected by employing the inverse heat conduction scheme.

On the back side of the test plate, the boundary condition was type I. The temperature of the back surface was set to the values read by two thermocouples on the back surface. In this study, since the Lexan substrate was selected to be thick enough as an insulator to reduce the back losses. The back surface temperature was able to be maintained at the ambient temperature during each experiment. This was verified by the two thermocouples mounted on the back surface.

On the other four surrounding sides of the test plate, adiabatic boundary condition was applied, which could be treated as a special case of type II boundary condition with zero heat flux input.

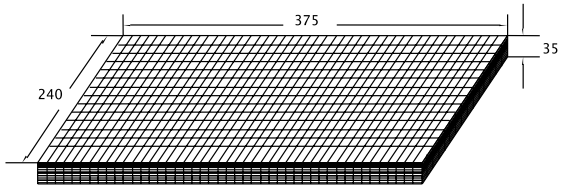

Fig. 7. Computational grid system.

The input information required for the calculation is listed below:

(1) the heat flux generated by the heater,
(2) thermophysical properties of the materials including the test surface, heater and the composite substrate,
(3) ambient temperature during the experiment,
(4) the boundary conditions on all the boundaries including the guessed heat transfer coefficients on the front surface,
(5) the initial condition of the entire computational domain,
(6) the dimensions of the test surface, and
(7) the grid system's configuration.

4.3. Experimental procedure

Before the experiments were conducted, the CCD camera was calibrated by using a standard color map to verify the digitization property and reliability of the particular camera used. A hardcopy of color map including the three primary colors was used as the reference. The CCD camera used for the heat transfer study was employed to record three images of the color map at different dates. The time interval between the taking of each image was 24 h. Those three images were then digitized by the image board and processed by the MATLAB image toolbox. The *RGB* values of each pixel of these different images were compared and found to be consistent within 1.3%. It was concluded that the camera was reliable to use.

A pre-test of the color property of the liquid crystal sheet was conducted on the target surface heated with a constant heat flux without air impingement. The pre-test indicated that the foil heater delivered an acceptable uniformity of heating. The temperature variation between any two randomly chosen locations on the surface (or pixels of the TLC images) at any time during measurement was found within 0.2 °C with a $\Delta T(= T_w - T_\infty)$ of 8 °C.

To minimize the deterioration of the color play properties of TLC sheet, the TLC surface was well covered and protected by a black card-board sheet and cloth immediately after each test. To eliminate errors due to lighting and viewing angle, an in situ calibration was performed for each experiment. In every test case, readings of three embedded thermocouples were used as the standard against which the color images were calibrated. The thermocouples themselves were calibrated against an RTD which was supplied and calibrated by National Institute of Standard and Technologies (NIST).

A heat transfer test was started about 20 min after the flow reached steady state by switching on the DC power supply of the heater. At the same time, the CCD camera and the thermocouple temperature measurement system were turned on. Three embedded thermocouple readings were matched by their physical (or real) time to produce the one-to-one relationship with the corresponding frame of the color image. By specifically looking at the hue angles of the TLC display at these three locations, a unique relationship between the temperature and the hue-angle was established for each thermocouple location. Ideally, for one specific temperature, the hue angle derived from the temperature data of three locations should be identical. For the four cases performed, the hue angle's variations were within 3%. The averaged calibration curve was used. The complete image change history during the transient tests was recorded by the CCD camera on an 8 mm tape, which

Table 1
*N*th order uncertainty analysis of heat transfer coefficient results

Independent variables	Nominal values	Uncertainty magnitudes	Individual uncertainty of h (%)
Main flow temp. (°C)	22.8	0.2	2.0
Initial temp. (°C)	22.8	0.2	1.0
Test surface thickness (mm)	13.8	0.025	1.8
Voltage (V)	75.0	0.51	1.0
Current (A)	0.35	0.02	1.2
Hue angle (°)	150	0.5	0.3
Test surface height (m)	0.1	0.0005	0.24
Test surface width (m)	0.18	0.0005	0.13
Thermal conductivity of Lexan (W/m °C)	0.193	0.5	0.09
Density of Lexan (kg/m^3)	2210.0	0.5	0.02
Specific heat of Lexan (J/kg °C)	1670.0	1.2	0.01
Thermal conductivity of silicon rubber (W/m °C)	0.150	0.020	0.003
Density of silicon rubber (kg/m^3)	1200.0	1.2	0.02
Specific heat of silicon rubber (J/kg °C)	2010.0	2.1	0.01
h (W/m^2 °C)	350	20.54	5.9 (total uncertainty)

acted as a raw data storage media. Typically, the test lasted from 4.5 to 7.5 min, depending on the test conditions such as heat flux levels and corresponding jet Reynolds numbers.

In the present experimental situation, since the heat transfer condition was transient, the effect of development of thermal boundary layer needed to be evaluated. Several different heating processes using different amounts of heating power were performed under the same flow condition (or Reynolds number). The experimental results showed differences within 1%, which is believed including the effect of thermal boundary layer development but not exclusively.

5. Uncertainty analysis

The uncertainty analysis was performed before, through, and after the experiment following the procedure proposed by Moffat [19]. The independent variables were traced and identified following the methodology proposed by Wang and Simon [20]. The result of N-th order uncertainty analysis is shown in Table 1. The detailed analysis including zeroth order, the first-order and the pre-test uncertainty analysis is documented by Lin [21]. The largest uncertainty (2%) is contributed by the 0.2 °C uncertainty in reading the mean flow temperature. The second largest uncertainty (1.8) is contributed by the uncertainty of 0.025 mm in reading the test surface thickness. The total uncertainty of the heat transfer coefficient is 5.9%. Initially, it was concerned that the uncertainty of hue angle might significantly contribute to the overall uncertainty. However, a careful execution of hue capturing and data processing, accompanied by in situ thermocouple calibration, have reduced the uncertainty of hue angle to approximately 0.3%.

6. Results and discussion

The transient TLC method has provided test results with remarkable spatial resolution for engineering

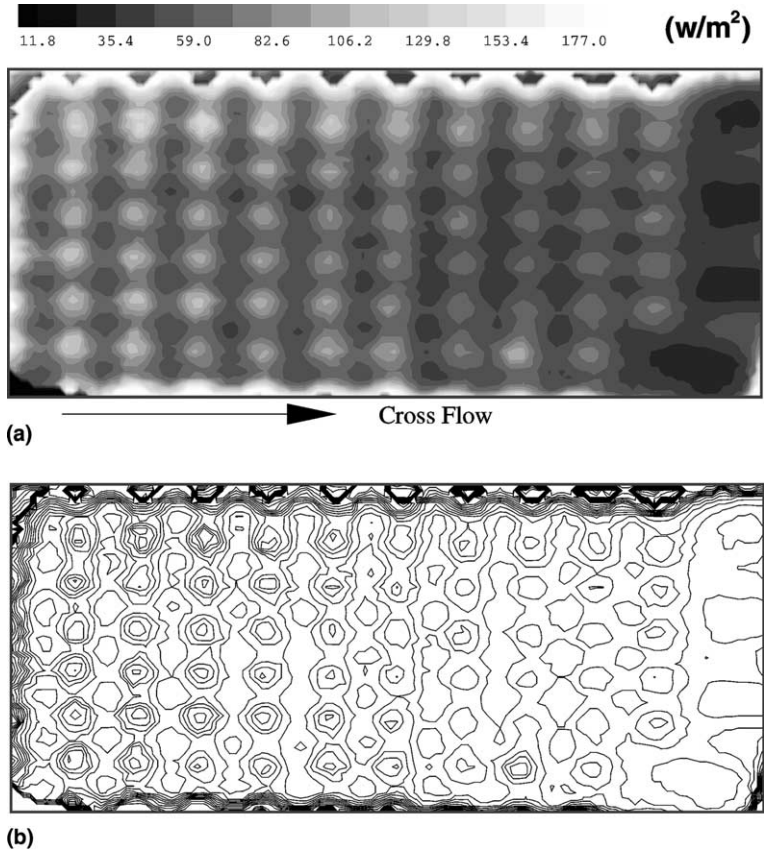

Fig. 8. Contour plot of convective heat transfer coefficient distribution (W/m² °C) on the impingement target surface with $Re = 1039$: (a) gray scales; (b) contour lines.

Table 2
Comparison between the 3-D and 1-D overall heat transfer results for one case at $Re = 1039$

Model	h_{min} (W/m^2 °C)	h_{max} (W/m^2 °C)	H (W/m^2 °C)	H/Re (W/m^2 °C)	Nu/Re
3-D	11.80	188.76	71.91	0.0692	0.00265
1-D	13.28	210.47	80.83	0.0778	0.00298

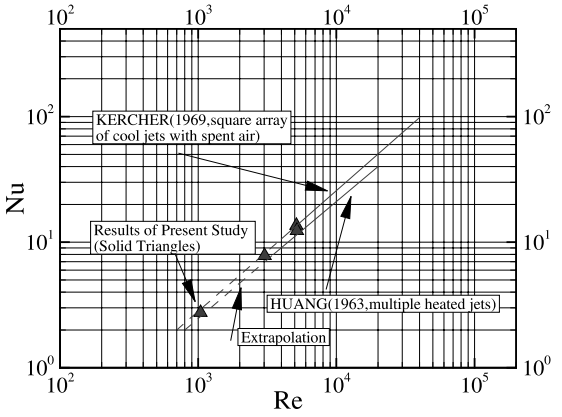

Fig. 9. Comparisons of the present experimental results with other studies. The dashed lines are extrapolations made by the present study.

needs. Each frame consisted of 480 × 752 pixel image that covered an actual viewing area of 10 cm × 16 cm (height × width).

In order to validate the present TLC method, experimental cases at $Re = 1039$, 3026, and 5133 were conducted to investigate the convective heat transfer coefficient distribution on the impingement surface. The results of $Re = 1039$ are shown in 2-D local heat transfer coefficient distribution in Fig. 8, presented by both gray scale and line contour plots. The average (H), maximum (h_{max}), and minimum (h_{min}) values of heat transfer coefficients over the entire target surface are shown in Table 2.

The results show that Nu/Re values are $0.00265 \pm 1\%$ or $Nu = 0.00304Pr^{0.42}Re$. The present results agree well with Kercher and Tabakoff's [22] correlations within 10% as shown in Fig. 9. They proposed $Nu/Pr^{1/3} = 0.00395Re^{0.966}$. They investigated heat transfer by a square array of round air jets impinging perpendicularly to a flat surface including the effects of spent air, which was similar to the present study. Their data cover a range of jet diameter Reynolds number from 300 to 30,000, jet spacing from 3.1 to 12.5 jet diameter, and plat-to-surface distance of 1.0–4.8 jet diameter. The comparisons are also made with the correlation proposed by Huang [23]. Huang investigated the heat transfer coefficients for airflow through round jets impinging normal to a heat transfer surface without spent air effects. This comparison validates the present method in a global scale, but the present results provide extremely detailed local heat transfer coefficient distribution which was obtained without approximations inherited in 1-D transient liquid crystal method.

A comparison between the 3-D and 1-D results for $Re = 1039$ is shown in Fig. 10. Fig. 10(a) shows the local heat transfer coefficient value (h) along a horizontal straight line through the centers of the fourth row of impingement holes. The 1-D results show that the local maximum and minimum values are approximately 15–20% higher than the 3-D results. To further compare the spanwise average of the results, the whole target surface

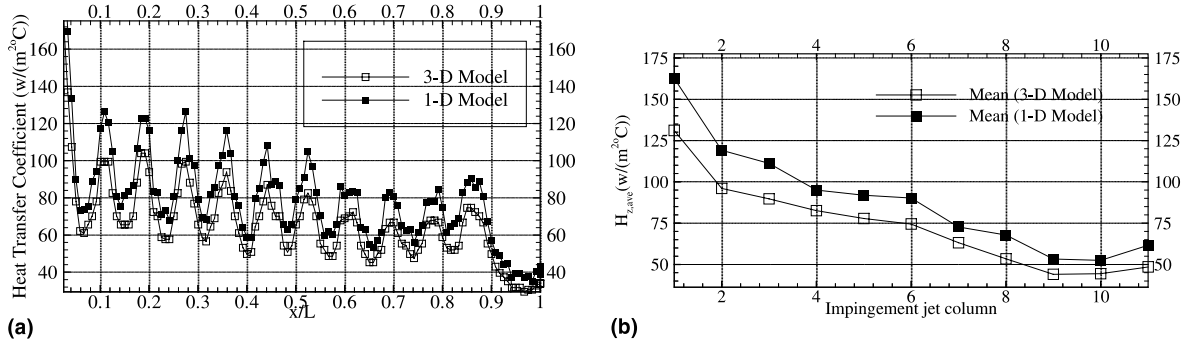

Fig. 10. Comparison between 3-D and 1-D results for $Re = 1039$: (a) local heat transfer coefficient along the center of the fourth-row of jet holes; (b) spanwise average of the heat transfer coefficients distribution.

is divided into 88 sub-domains (8 rows × 11 columns) with the jet-hole location placed in the middle of each sub-domain. The measurement was made from a 240 × 376 array of pixels; therefore, each sub-domain contains 30 × 34 measurement points. Fig. 10(b) shows that the 1-D result of the spanwise average heat transfer coefficient (H_z) for each column is approximately 20% higher than the 3-D results. Comparison of the overall average of the heat transfer coefficient (H) between 1-D and 3-D results, as shown in Table 2, indicates that 1-D method over-predicts the heat transfer coefficient about 12%. This can be explained that 3-D method accounts for the lateral heat flows induced by local temperature gradients, which smear out the heat transfer effect. A detailed analysis of the present results, together with other three experimental cases, is presented by Wang et al. [24].

7. Conclusions

A transient liquid crystal method was developed and validated by conducting an experimental investigation of heat transfer and flow structure of impingement jet arrays in a confined space.

Instead of utilizing the conventional 1-D transient TLC method, the present study employed a new transient liquid crystal method coupled with an inverse 3-D transient conduction scheme. Hue angle method was first time-employed in a transient liquid crystal scheme by the present study to achieve better certainty for mapping temperature versus color relationship. Synchronized temperature readings from embedded thermocouples are used for in situ calibration. Merits for adopting the present method include: (1) reducing the complexity of the experimental procedures and experimental set up by avoiding imposing instantaneous step-change of heated/cooled flow (2) replacing 1-D approximation with more accurate 3-D computation, and (3) replacing unsteady flow condition with steady flow condition.

The results indicate that the 1-D results are higher than the 3-D results with the local maximum and minimum heat transfer values being over-predicted by about 15–20% and the overall heat transfer by approximately 12%. This is due to the fact that 1-D method does not include the local lateral heat flow induced by local temperature gradients.

Acknowledgements

The authors want to thank Dr. Ronald S. Bunker of General Electric Corporate R & D for providing technical support to this project.

References

[1] J.L. Ferguson, Liquid crystals in non-destructive testing, J. Appl. Opt. (7) (1968) 1729–1737.
[2] C. Den Ouden, C.J. Hoogendoorn, Local convective heat transfer coefficients for jets impinging on a plate: experiments using a liquid crystal technique, in: Proceedings of the 5th Heat Transfer Conference, New York, vol. 5, 1974, pp. 293–295.
[3] T.E Cooper, R.J. Field, J.F. Meyer, Liquid crystal thermograph and its applications of the study of convective heat transfer, ASME J. Heat Transfer (97) (1975) 442–450.
[4] R.J. Goldstein, J.F. Timmers, Visualization of heat transfer from arrays of impinging jets, Int. J. Heat Mass Transfer (25) (1982) 1857–1868.
[5] N. Akino, T. Kunugi, K. Ichimiya, K. Mitsushiro, M. Ueda, Improved liquid crystal thermometry excluding human color sensation, ASME J. Heat Transfer (111) (1989) 558–565.
[6] J.W. Baughn, A.E. Hechanova, X. Yan, An experimental study of entrainment effects on the heat transfer from a flat surface to a heated circular impingement jet, ASME J. Heat Transfer (113) (1991) 1023–1025.
[7] J.C. Simonich, R.J. Moffat, A New technique for mapping heat transfer coefficient contours, Rev. Sci. Instrum. (53:5) (1982) 678–683.
[8] S.A. Hippensteele, L.M. Russell, F.J. Torres, Use of a liquid-crystal and heat element composite for quantitative, high-resolution heat transfer coefficients on a turbine airfoil including turbulence and surface-roughness effects, pressure and temperature measurements, ASME WAM (1986) 105–120.
[9] N. Arkno, T. Kunugi, K. Ichimiya, A. Kurosawa, Liquid-crystal thermometry based on automatic color evaluation and applications to measure turbulent heat transfer, in: Proceedings of the Second International Symposium on Transport Phenomena in Turbulent Flows, Tokyo, 1987, pp. 627–640.
[10] D.K. Hollingsworth, A.L. Boehman, E.G. Smith, R.J. Moffat, Measurement of temperature and heat transfer coefficient distributions in a complex flow using liquid crystal thermograph and true-color image processing, J. Heat Transfer (123) (1989) 35–42.
[11] C. Camci, K. Kim, S.A. Hippensteele, Evaluation of a hue capturing based transient liquid for high-resolution mapping of convective heat transfer on curved surfaces, ASME J. Heat Transfer 2 (1993) 311–318.
[12] P.T. Ireland, T.V. Jones, Detailed measurements of heat transfer on and around a pedestal in fully developed channel flow, in: Proceedings of 8th International Heat Transfer Conference, San Francisco, 1986, pp. 975–986.
[13] D.E. Metzger, R.S. Bunker, G. Bosch, Transient liquid crystal measurement of local heat transfer on a rotating disk with jet impingement, J. Turbomachinery (113) (1991) 52–59.
[14] A.M. Humber, R. Viskanta, Effect of jet-jet spacing on convection heat transfer to confined, impinging arrays of axis-symmetrical air jets, Int. J. Heat Mass Transfer (37) (1994a) 2859–2869.
[15] M.K. Chyu, H. Ding, J.P. Downs, A. van Sutendael, F.S. Soechting, Determination of local heat transfer coefficient

based on bulk mean temperature using a transient liquid crystals technique, 1997, ASME paper 97-GT-489.
[16] S.V. Ekkad, J.C. Han, Detailed heat transfer distributions in two-pass square channels with Rib turbulators, Int. J. Heat Mass Transfer 40 (11) (1997) 2525–2537.
[17] W.N. Sponson, in: Color Science in Television and Display System, Adam Hilgter Ltd., Bristal, 1983, pp. 1–59.
[18] W.K. Pratt, in: Digital Image Processing, Wiley, New York, 1978, pp. 50–90.
[19] R.J. Moffat, Contributions to the theory of single-sample uncertainty analysis, J. Fluids Eng. (104) (1982) 250–260.
[20] T. Wang, T.W. Simon, Development of a special purpose test surface guided by uncertainty analysis, AIAA J. Thermophys. Heat Transfer 3 (1) (1989) 1926.
[21] M. Lin, Flow and heat transfer of confined impingement jets, MS Thesis, Department of Mechanical Engineering, Clemson University, USA, 1999.
[22] D.M. Kercher, W. Tabakoff, Heat Transfer by a square array of round air jets impinging perpendicular to a flat surface including the effect of spent air, ASME J. Eng. Power (1970) 73–83.
[23] P.G. Huang, A.S. Mujumdar, W.J. Douglas, Numerical prediction of fluid flow and heat transfer under a turbulent impinging slot jet with surface motion and crossflow, 1984, ASME paper 84-WA/HT-33.
[24] T. Wang, M. Lin, R.S. Bunker, Flow and heat transfer of confined impingement jets cooling, 2000, ASME paper GT-00-223.